PERGAMON

International Journal of Solids and Structures 38 (2001) 5545–5563

INTERNATIONAL JOURNAL OF SOLIDS and STRUCTURES

www.elsevier.com/locate/ijsolstr

Finite crack kinking and *T*-stresses in functionally graded materials

T.L. Becker Jr. [a], R.M. Cannon [b], R.O. Ritchie [b,*]

[a] *Salomon Smith Barney, Fixed Income Research, New York, NY 10013, USA*

[b] *Materials Sciences Division, Lawrence Berkeley National Laboratory, Department of Materials Science and Engineering, University of California, Berkeley, CA 94720, USA*

Received 12 June 2000; in revised form 16 October 2000

Abstract

The optimum direction of in-plane continuous crack advance in functionally graded materials (FGMs) is discussed. The FGM is modeled using finite element analysis as a linear elastic material with spatially varying Young's modulus. The kink direction was determined as the angle at which either the energy release is maximized (G_{max}) or at which the kink tip is deformed without shear ($K_{II} = 0$). Results are found to asymptote toward that from the infinitesimal short kink analyses for homogeneous materials, based on the local gradient-adjusted phase angle but only for very short kinks. The systematic discrepancy between the finite and infinitesimal results can be accounted for by including the effect of the apparent parallel *T*-stress. This *T*-stress is affected by both the far-field parallel loading and, unlike in homogeneous materials, the far-field phase angle. The magnitude of the *T*-stress is, on average, greater than that for the identical geometry comprised of a homogeneous material. For kink lengths of the same order of the gradient dimension and greater, there is a divergence between the kink angles for the two criteria. In addition, there is a bifurcation in the G_{max} results for negative far-field phase angles. This is caused by the competition between the near-tip *K*-dominant field and the nonsingular gradient-induced terms, which, in turn, reflects differing effects of the far-field loading and the tendency of the crack to move toward the more compliant region within the modulus gradient. © 2001 Published by Elsevier Science Ltd.

Keywords: Fracture; Crack kinking; Functionally graded materials; *T*-stress

1. Introduction

Developing applications in aerospace, power generation, microelectronics and bioengineering demand properties that are often unobtainable in any single material. Correspondingly, composite or layered materials are often developed to invoke the desirable characteristics of each of the constituent phases in order to meet such requirements. However, the internal stresses caused by the elastic and thermal properties mismatch at an interface between two differing bulk materials can mitigate the successful implementation of

* Corresponding author. Tel.: +1-510-486-5798; fax: +1-510-486-4881.
E-mail address: roritchie@1bl.gov (R.O. Ritchie).

0020-7683/01/$ - see front matter © 2001 Published by Elsevier Science Ltd.
PII: S0020-7683(00)00379-6

Nomenclature

$f_{\mathrm{I}}(\theta), f_{\mathrm{II}}(\theta)$ nondimensional functions relating stress to angle
x, y Cartesian coordinates
r, θ polar coordinates
$a, \Delta a$ crack length, kink length
ω kink angle
K_1, K_2 stress intensity factors for unkinked straight crack
$K_{\mathrm{I}}, K_{\mathrm{II}}$ stress intensity factors at tip of crack kink
T, T_b homogeneous, FGM T-stress
$A_{\mathrm{I,II}}, B_{\mathrm{I,II}}$ coefficients relating stress intensities of main crack to those of a kink
$C_{\mathrm{I,II}}$ coefficients relating T-stress and kink length to stress intensities of a kink
ψ, ψ^{∞} tip, far-field phase angle, $\psi = \tan^{-1}(K_2/K_1)$
$G^{\Delta a}$ energy release rate for kink with length Δa
G infinitesimal energy release rate, $\Delta a \to 0$
σ_{xx}, σ_{yy} normal planar Cartesian stresses
$\sigma_{\theta\theta}, \sigma_{r\theta}$ hoop, shear stress in polar coordinates
$\delta_{\theta}, \delta_r$ crack opening, sliding displacements
$\omega_{\sigma\theta\theta,\max}$ optimum kink angle via $\sigma_{\theta\theta,\max}$ criterion
$\omega_{K_{\mathrm{II}}=0}(\Delta a)$ optimum kink angle via $K_{\mathrm{II}} = 0$ criterion
$\omega_{G_{\max}}(\Delta a)$ optimum kink angle via $G_{\max}$ criterion
E, ν Young's modulus, Poisson's ratio
E_0, E' homogeneous modulus, plane strain modulus $= E/(1-\nu^2)$
$\alpha, \beta; \varepsilon$ bimaterial Dundurs' parameters; oscillatory index
L reference distance for interface phase angle
b, c modulus slope and crack-tip value parameters, where $E(y) = (c-1)\tanh(by) + c$
$B_{\varepsilon}, B_{\sigma}$ deformation, stress biaxiality
r_K K-dominant region size
W work to close kinked crack per unit thickness
$1/M$ fraction of kink over which work is integrated analytically
$\overline{\sigma}_{r1}, \overline{\sigma}_{\theta 1}$ coefficients used to approximate the Williams' singular stress field
$\overline{\delta}_{(r,\theta)(1,2)}$ coefficients used to approximate linear crack opening displacements
$\varepsilon_{yy}^{\infty}\ \varepsilon_{xx}^{\infty}\ \varepsilon_{xy}^{\infty}$ far-field nominal strains
$\sigma_{xx}^{\infty}\ \sigma_{yy}^{\infty}\ \sigma_{xy}^{\infty}$ far-field nominal stresses
w width of square sheet geometry
$|K|$ magnitude of stress intensity factors, $(K_{\mathrm{I}}^2 + K_{\mathrm{II}}^2)^{1/2}$

such composites. To address this problem, functionally graded materials (FGMs) have been developed to satisfy the needs for properties that are unavailable in any single material and for graded properties to offset the adverse effects of discontinuities.

The introduction of continuous compositional changes removes large-scale interface-stress singularities and can even result in stress-free material joints. This gradual change in composition over length scales that are significant in comparison to the overall dimensions of the body is what distinguishes FGMs from other composites. The shape of this gradient is an additional parameter determining the behavior of an FGM structure. Associated complications involving spatially varying elastic constants have demanded the re-examination of the elastic crack problem. Although the fracture mechanics solutions for stress and dis-

placement fields in homogeneous and graded materials agree in the asymptotic near-tip limit (Erdogan, 1995; Jin and Noda, 1994), the scope of the material gradient effects on fracture behavior are not fully comprehended.

For cracks loaded in tension and shear, the direction of crack growth is an important aspect of fracture behavior. For FGMs with variable modulus, mixed-mode cracks are common (Konda and Erdogan, 1994). In this paper, we present an analysis of the kinking problem for FGMs that incorporates both traditional fracture mechanics parameters and higher-order terms in the stress field, which depend on the gradient. This approach is used to permit the calculation of the optimum crack path given the loading and material parameters.

2. Crack kinking in homogeneous materials

Historically, fracture mechanics research first sought to determine the conditions for stability of straight cracks extending in their own plane. For mixed-mode loading, this is often not the mechanically or energetically most favorable path. In fact, a variety of methodologies have been employed to determine the direction of crack growth under mixed-mode (tensile and shear) loading in homogeneous and layered materials.

The first calculations were those of Erdogan and Sih (1963), who developed the criterion that the crack will grow in the direction along the angle, ω, of maximum $\sigma_{\theta\theta}$ (hoop stress) near the tip of the preexisting (unkinked) crack in a linear elastic material. Using the K-field solution of Williams (1957), the optimal in-plane kink angle $\omega_{\sigma\theta\theta,\max}$ can be calculated as the solution to

$$K_1 \sin(\omega) - K_2(3\cos(\omega) - 1) = 0. \tag{1}$$

The analysis of the problem was advanced to include the geometry of a small off-plane extension (kink) (Fig. 1). The stress intensity state $(K_{\mathrm{I}}, K_{\mathrm{II}})$ of a kink can be calculated in terms of the stress field surrounding the tip of the original crack (with stress intensities K_1, K_2). Using analysis of Erdogan and Sih (1963), the subsequent direction of crack growth can be determined. Utilizing the power series description of the each component of stress near the unkinked crack,

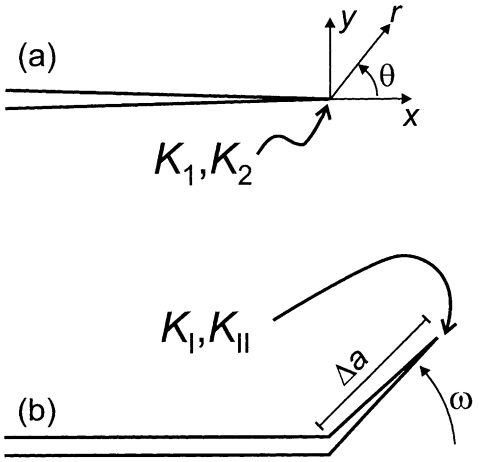

Fig. 1. Schematic of straight (a) and kinked (b) cracks. The state at the tip of the unkinked crack is characterized by stress intensities K_1, K_2. The kink at angle ω to the $y = 0$ plane with length Δa is characterized by K_{I}, K_{II}.

$$\sigma = \frac{K_1 f_1(\theta) + K_2 f_{II}(\theta)}{\sqrt{2\pi r}} + T + O(r^{1/2}) \tag{2}$$

the role of the coefficients (K_1, K_2, T, and those of the $r^{1/2}$ and $r^{3/2}$ terms) describing the stress state near the crack in determining the tendency of a kink to grow increasingly away from $y = 0$ (or to return to the original crack plane) was established (Cotterell, 1966).

The second term represents the strength of a constant stress expressed only in the xx component, σ_{xx}, and is usually referred to as the T-stress. The T-stress is, in general, independent of the stress intensity factor; that is, two cracked bodies can have the same K_1, K_2, but different Ts. For a mode-I ($K_2 = 0$) crack, a negative (compressive) value of T stabilizes the crack path. For a positive (tensile) T-stress, the path is destabilized; that is, if a small random kink is formed along a positive angle ω, subsequent crack growth will occur at an angle greater than ω. Similar analysis was performed on curved cracks (Cotterell and Rice, 1980). Both are approximations that are only accurate to the first order of ω.

For analysis of kinks at finite angles, the stress intensity factors at the tip of the kink were determined for cracks on sharp interfaces and in homogeneous materials by He and Hutchinson (1989) and He et al. (1991). Here the stress intensity factors for a kink of length Δa are calculated in the form

$$K_I = A_I K_1 + B_I K_2 + C_I T\sqrt{\Delta a}, \tag{3a}$$

$$K_{II} = A_{II} K_1 + B_{II} K_2 + C_{II} T\sqrt{\Delta a}, \tag{3b}$$

where K_1 and K_2 are the stress intensity factors of the unkinked crack tip (Fig. 1). For homogeneous materials, approximately equivalent coefficients $A_{I,II}$ and $B_{I,II}$ are also given in the earlier work of Hayashi and Nemat-Nasser (1981). The strain energy release rate of the kink can subsequently be calculated via $G = (K_I^2 + K_{II}^2)/E'$. Using the tip state, the angle for which $G(\omega)$ is maximized can be calculated from K_1, K_2, and T. Alternately, the angle at which $K_{II}(\omega) = 0$ can be determined.

The $K_{II} = 0$ criterion can be understood from a symmetry argument. For brittle materials, failure is associated with normal (rather than shear) stresses. A crack growing in mixed mode would be growing into combined tensile and shear stress field. Therefore, the kink in pure mode-I is the only stable path. However, for finite-length straight cracks, this criterion has less appeal, as it focuses solely on the conditions near the tip of the kink. The G_{max} formulation of the problem suppresses any influence of the mechanism of crack advance, but instead appeals to the variation principle for linear elasticity.

Palaniswamy and Knauss (1978) used Betti's reciprocal theorem to explain the close agreement of the two methodologies. The energy release rate, G, can be written as

$$G(\omega) = \lim_{\Delta a \to 0} \frac{1}{2\Delta a} \int_0^{\Delta a} \left(\sigma'_{\theta\theta}(r,\omega)\delta''_{\theta}(r,\omega) + \sigma'_{r\theta}(r,\omega)\delta''_{r}(r,\omega) \right) dr, \tag{4}$$

where $(\,)'$ denotes the unkinked solution (Fig. 1a), $(\,)''$ the kinked (Fig. 1b), and δ the opening displacements across the kink faces. The G_{max} criterion is satisfied by the combined effect of both of the integrals, where as the $K_{II} = 0$ criterion infers restrictions on the stress term in the second integral.

A comparison of the stress intensity and energy criteria for the optimal kink angle can be found in He and Hutchinson (1989) (Fig. 2); the two methodologies agree at phase angle $\psi = \tan^{-1}(K_{II}/K_I) = 0°$ (pure tension, $K_{II} = 0$) and diverge by about 3° at $\psi = 90°$ (pure shear, $K_I = 0$). Cotterell (1965) showed the equivalence of the direction of maximum hoop stress prediction with that of maximum energy release for small ω. The agreement for large ω is surprisingly good. Experimental evidence clearly shows the advantage of the finite ω calculations (Eqs. (3a) and (3b)) over $\omega_{\sigma\theta\theta,max}$ (Finnie and Saith, 1973), but the scatter is sufficiently large that discriminating between the $K_{II} = 0$ and G_{max} criteria is difficult.

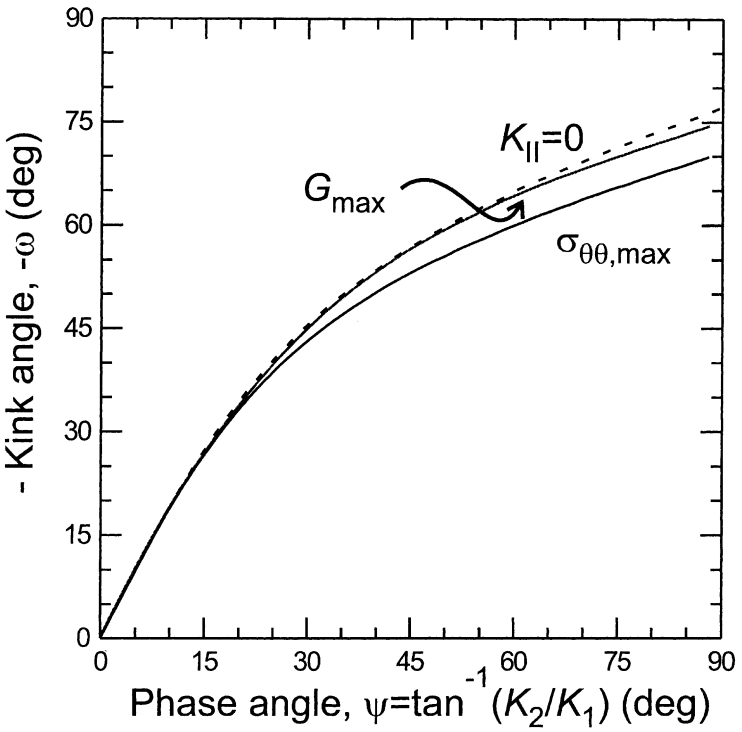

Fig. 2. Comparison of three theories for optimal crack kinking angle in homogeneous materials. Predicted kink angles are based on loading phase angles ψ. Up to $\omega \sim 45°$, they all agree within 5°. Maximum stress criterion, $\sigma_{\theta\theta,\max}$ is based solely on the stress state before kinking. The $K_{II} = 0$ criterion dictates that kinks will grow only in a state of pure crack tip tension. The maximum energy release rate criterion, $G_{\max}$, selects paths based on a global reduction in energy.

3. Crack kinking in functionally graded materials

FGMs, like discrete elastic interfaces, are inherently prone to developing mixed-mode cracks. Nevertheless, few studies on crack kinking in FGMs have been performed. Lee and Erdogan (1995) calculated the effect of modulus gradient on the angle of maximum hoop stress near the free edge of a graded joint and discussed the implications on the direction of fracture initiation. The coincidence of the asymptotic stress solution of the crack problem with the homogeneous solution of Williams (1957) motivated Gu and Asaro (1997) to apply the analysis of Cotterell and Rice (1980) to various geometries with modulus gradients. This analysis inherits the approximation for suitably small kink angles. Furthermore, it assumes no gradient effect on the kinking behavior besides that which is characterized in the near-tip phase angle ψ. The direction of crack growth will vary from this prediction for any nonzero length. The authors, however, give no guidance as to the range over which this analysis will be accurate.

4. Problem formulation

4.1. Kinked crack geometry

To assess the dependence of the optimal kink angle on kink length, a finite geometry with various combinations of kink angle and length was analyzed. Ideally, the far-field boundary conditions should be

set such that the results are the most general. For instance, in studying crack kinking behavior of a nonlinear elastic material, Geubelle and Knauss (1995) employed a boundary layer methodology where the far-field boundary conditions were assigned to be those of the linear elastic crack solution. The body was large enough so that the distance to the boundary did not effect the outcome of the solution. This is the familiar small-scale yielding condition. Such results could be applied to any body large enough that it could be expected to contain a sufficiently large linear K-dominant zone.

Such a methodology presupposes a nested set of singular solutions, namely that a nonlinear field is bounded by linear K-field. No such set of solutions is known for an FGM. However, as shown in the work of Jin and Batra (1996), the gradient-induced terms should be important in the neighborhood near the crack tip such that $r \sim 1/b$ (where b is the gradient dimension, obtained from the modulus variation, Eq. (9)). For a homogeneous linear body, the K-dominant region of size r^K should scale with about 1/10 to 1/100 of the smallest in-plane dimension. Therefore, for $r \sim 1/b \ll r_K^{\text{hom}}$ the stress state should be characterized by crack tip ($\mathrm{O}(r^{-1/2})$) and other gradient-induced terms. For $r < r_K^{\text{FGM}} \ll 1/b$ the stress state is describable by K_1 and K_2 alone.

The geometry analyzed was a square sheet with a centered crack with length $2a$ (Fig. 3) and an in-plane kink of length Δa. The outer dimensions are much greater than the crack length, with a width-to-crack length ratio $w/a = 20$. Therefore, the details of the size and shape of the boundary are of minimal consequence to the near-tip conditions. [1] The tip and kink regions are refined (Fig. 4) to accurately model the stress singularities. Solutions were obtained with the finite element package FEAP (Zienkiewicz and Taylor, 1989) with linear elastic elements that allowed for inter-element variation of the Young's modulus, E. (Variations in the Poisson's ratio v are also possible, but were not included in this study.) Meshes consisted of 10,000–13,000 quadrilateral plane-strain elements.

The edges of the sheet have set displacements. The deformation is characterized by the linear strain that would occur in a homogeneous crack-free sheet normal to the plane of the crack, $\varepsilon_{yy}^{\infty}$, parallel to the crack, $\varepsilon_{xx}^{\infty}$, and in shear, $\varepsilon_{xy}^{\infty}$. The corresponding reference stresses scale with a homogeneous modulus E_0 and are

$$\sigma_{xx}^{\infty} = E_0 \frac{\varepsilon_{xx}^{\infty}(1-v) + v\varepsilon_{yy}^{\infty}}{1 - v - 2v^2},$$

$$\sigma_{yy}^{\infty} = E_0 \frac{\varepsilon_{yy}^{\infty}(1-v) + v\varepsilon_{xx}^{\infty}}{1 - v - 2v^2}$$

and

$$\sigma_{xy}^{\infty} = \frac{E_0 \varepsilon_{xy}^{\infty}}{(1+v)}.$$

The biaxiality of the deformation B_ε is the ratio of the normal strain in the x-direction to that in the y-direction, $\varepsilon_{xx}^{\infty}/\varepsilon_{yy}^{\infty}$ and can be related to the biaxiality of the reference stress through

$$B_\sigma = \frac{\sigma_{xx}^{\infty}}{\sigma_{yy}^{\infty}} = \frac{B_\varepsilon(1-v) + v}{(1-v) + vB_\varepsilon}.$$

The far-field (or reference) phase angle is defined as $\psi^{\infty} = \tan^{-1}(\sigma_{xy}^{\infty}/\sigma_{yy}^{\infty})$. For a homogeneous material, the phase angle at the tip of a crack $\psi = \tan^{-1}(K_{\mathrm{II}}/K_{\mathrm{I}}) = \psi^{\infty}$. However, for graded structures, there is a shift in the phase angle corresponding to gradient strength (Erdogan, 1995). Furthermore, for homogeneous materials the T-stress is a linear function of the stress biaxiality, B_σ. Less well understood is the nature of the T-stress for FGMs.

[1] Analysis of a sheet with $W/a = 40$ yielded results for kink angles within 0.2° of those for $W/a = 20$.

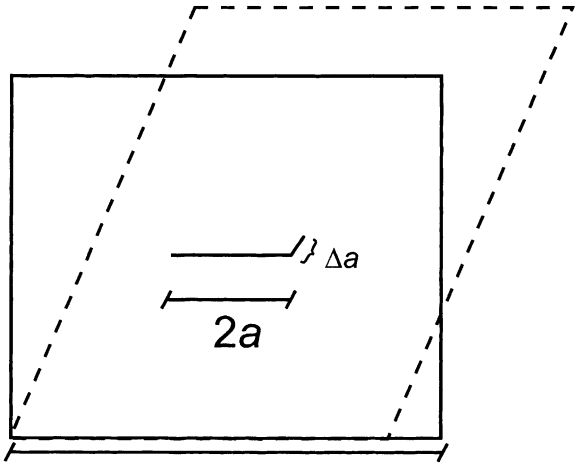

Fig. 3. Schematic of the problem studied: a cracked sheet undergoing normal and shear deformation. Displacements were fixed on all boundaries and loading characterized by the apparent normal and shear strains, $\varepsilon_{xx}^{\infty}$, $\varepsilon_{yy}^{\infty}$ and $\varepsilon_{xy}^{\infty}$. The crack was small compared to the sheet, $w/a = 20$, and the kink was smaller than the crack, $10^{-4} < \Delta a/a < 0.3$.

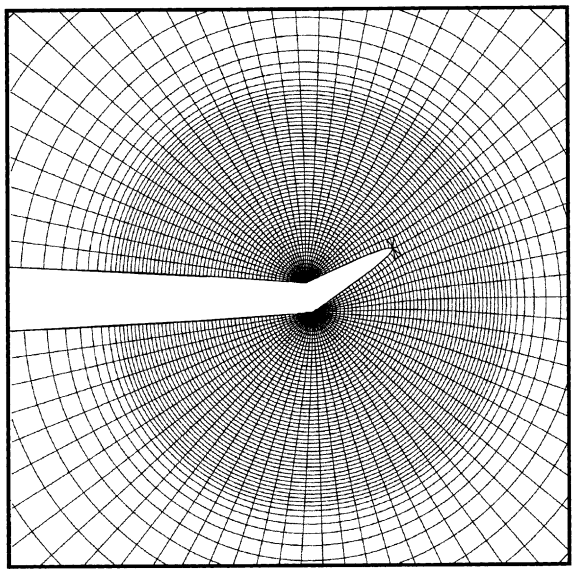

Fig. 4. Detail of the finite element mesh near the kinked crack. Refinement was employed to capture the details of the stress singularities. The fan array set elements every 5° with 20 elements positioned along the length of the kink. An eight-element fan was meshed at the tip of the kink.

4.2. Kink angle selection methodologies

4.2.1. Maximum energy release rate criterion

The energy release rate, G, is derived from the work, W, necessary to close the kink. This uses the stresses, σ, of the unkinked solutions and the crack opening displacements δ of the kinked solution (schematically, using two meshes corresponding to the geometries in Fig. 1a and b) via

$$W = \int_0^{\Delta a} \left(\sigma'_{\theta\theta} \delta''_{\theta} + \sigma'_{r\theta} \delta''_{r} \right) \mathrm{d}r. \tag{5}$$

Given the spatially discrete nature of the finite element solution, the nodal stresses and displacements are used as integration points to numerically evaluate Eq. (5); however, the linear elastic stresses at the root of the kink ($r = 0$) are infinite. Therefore, the stresses at those nodes cannot be directly used in a numerical integration. (The FEA *will* report finite stress values, but they will be mesh dependent.) The integration along the kink is divided into two parts, one to be solved analytically (from $r = 0$ to $\Delta a/M$) and one numerically (from $r = \Delta a/M$ to Δa). The stresses and analytical calculations were performed over the two elements closest to the kink root; this corresponds to an M of 12.5 for the kink modeled with 25 elements.

For the analytical calculation of the work, approximations are made for the stress behavior for the unkinked crack and the opening displacements for the kinked crack. Near the origin of the unkinked crack, the stress is assumed to behave as a Williams' singularity. Near the tip of the kinked crack, opening displacements scale with $\sqrt{(\Delta a - r)}$, but near $r = 0$ they can be seen to be approximately linear. The work is therefore an integral of the product of the singular (unkinked) stresses and the linear kink face opening:

$$W\left(r = 0 \text{ to } \frac{\Delta a}{M} \right) = \int_0^{\Delta a/M} \left(\frac{\overline{\sigma_{r1}}}{\sqrt{r}} \left(\overline{\delta_{r1}} + \overline{\delta_{r2}} r \right) + \frac{\overline{\sigma_{\theta 1}}}{\sqrt{r}} \left(\overline{\delta_{\theta 1}} + \overline{\delta_{\theta 2}} r \right) \right) \mathrm{d}r. \tag{6}$$

The values for $\overline{\sigma}_{r1}$, $\overline{\sigma}_{\theta 1}$, which scale the singular unkinked stresses, are fit from the stresses from the third and fourth elements from the crack tip (as the two elements neighboring a singularity are not considered to be accurate (Williamson et al., 1995)). $\overline{\delta}_{(r,\theta)(1,2)}$ are fit from the kinked solution displacements. The work over the remainder of the length (from $r = \Delta a/M$ to Δa) is integrated using Simpsons rule and the nodal values from stress and displacement.

The formal definition of the strain energy release rate, G, refers to the change in potential in the small crack limit (Eq. (4)). In the absence of additional work, that is under "fixed grip" conditions, this can be equated with a change in the work necessary to close the crack, $G = 1/2(\partial W/\partial a)$. A finite kink energy release rate is defined by, $G^{\Delta a} \equiv W/2\,\Delta a$; clearly as $\Delta a \to 0$, $G^{\Delta a} \to G$. When comparing kinks with different angles, this methodology yields the angle at which a kink of a given length, Δa, is most energetically favorable to form. This will be referred to as the $G_{\max}$ angle, $\omega_{G_{\max}}$.

4.2.2. Pure opening mode criterion

To determine the phase angle of the kink, the crack opening displacements were fit using the known near-tip behavior:

$$\delta_{\theta} + \mathrm{i}\delta_{r} = \frac{\sqrt{\Delta a - r}}{E'} (K_{\mathrm{I}} + \mathrm{i}K_{\mathrm{II}}) \tag{7}$$

such that

$$\psi^{\Delta a} = \arctan\left(\frac{\delta_r}{\delta_{\theta}} \right). \tag{8}$$

The displacements of the second element behind the tip of the kink are fit to Eq. (7) and the phase angle calculated. Note, that as the $G_{\max}$ criterion is integrated over Δa, the results reflect conditions along the entire kink length, but the $K_{\mathrm{II}} = 0$ criterion only depends on conditions near the tip of the kink.

4.3. Procedures

For each far-field phase angle, $\psi^{\infty} = 45°$, 0°, −45° and deformation biaxiality $B_{\varepsilon} = \{1, 0, -1\}$, kink lengths of $\Delta a/a = \{10^{-4}, 10^{-3}, 3\times10^{-3}, 10^{-2}, 3\times10^{-2}, 10^{-1}, 3\times10^{-1}\}$ are analyzed. In addition to the homogeneous case, a sigmoidal gradient in Young's modulus was assumed for analysis, where

$$E(y) = (c-1)\tanh(by) + c. \tag{9}$$

In the plane of the crack, $E = c$. The slope of the modulus function, $b(c-1)$, is controlled by b for fixed crack-tip value, c, which was set to be 10.5 for the analyses. This allows for a 20-fold change in the Young's modulus. The modulus gradient parameter is fixed, $b = 100/a$. Ninety percent of the change occurs over a distance $\sim 3/b$ and $\nabla E/E(0) = b(c-1)/c \approx b$. In the limit of $b \to \infty$, a sharp interface is formed, with $E(\infty)/E(-\infty) = 2c - 1$. Poisson's ratio, v, was taken be 0.3 for all cases.

A family of kink angles was analyzed for each phase angle and kink length, from values of ω from −85° to +85° in increments of 5°. For each kink angle, the work and kink-tip phase angles were calculated. A parabola was fit to the angles with the three largest $G^{\Delta a}(\omega)$. The angle corresponding the maximum of that parabolic equation was identified as $\omega_{G_{\max}}(\Delta a)$. The two points with phase angles closest to 0 were also selected and $\omega_{K_{\mathrm{II}}=0}(\Delta a) = 0$ linearly interpolated.

5. Results and discussion

5.1. Homogeneous material kink angles

The optimal kink angles predicted by the two criteria are displayed in Fig. 5a for a homogeneous material with phase angle $\psi^{\infty} = 45°$ and 75° and $B_{\varepsilon} = 0$. Solid lines indicate the predictions under the $G_{\max}$ criterion: −56.6° and −69.3° respectively. Dashed lines show that for the $K_{\mathrm{II}} = 0$ criterion: –57° and –71.5° (Hutchinson and Suo, 1991). These analyses assume an infinite K-field and are therefore independent of the length scale of the kink, Δa. This independence has been confirmed numerically by Geubelle and Knauss (1995).

The finite element analysis results show excellent agreement with the analytical solutions for the smallest kink lengths $\Delta a/a = 10^{-4}$ to 10^{-3}. For longer kink lengths, there is a monotonic deviation of the finite element results from the analytical results. This is due to the influence of finite geometry, primarily the T-stress. For both phase angles, $T/(K_1/\sqrt{a}) = -0.2$.

This negative T-stress stabilizes a straight-ahead crack (Cotterell, 1965), which corresponds to a decrease in the optimal ω. This effect will be quantified in subsequent sections. The deviation of these numerical results from the infinitesimal kink theories exhibit a kink-length effect due simply to pure finite geometry effects and will be used for comparison with the graded material results.

For $\psi^{\infty} = 0°$ and 45°, the finite kink energy release calculated for extension along $\omega = 0$ are shown in Fig. 5b. The results are compared to the analytical $G = (K_1^2 + K_2^2)^{1/2}/E'$, which holds in a pure K-field. There is no change in the results from $\Delta a/a = 10^{-4}$ to 10^{-2}, but as in Fig. 5a, there is a change between $\Delta a/a = 10^{-2}$ and 10^{-1}. This corresponds to the approximate size of the K-dominant region, $r_K = a/10 - a/100$ (Knott, 1973). The offset seen, ~1% for $\psi^{\infty} = 0°$ and 2% for $\psi^{\infty} = 45°$, is due to the approximate nature of the finite element results, which will always under-predict the displacements. This offset error could be reduced most effectively with additional mesh refinement, with a secondary benefit from a higher-order integration of Eq. (5).

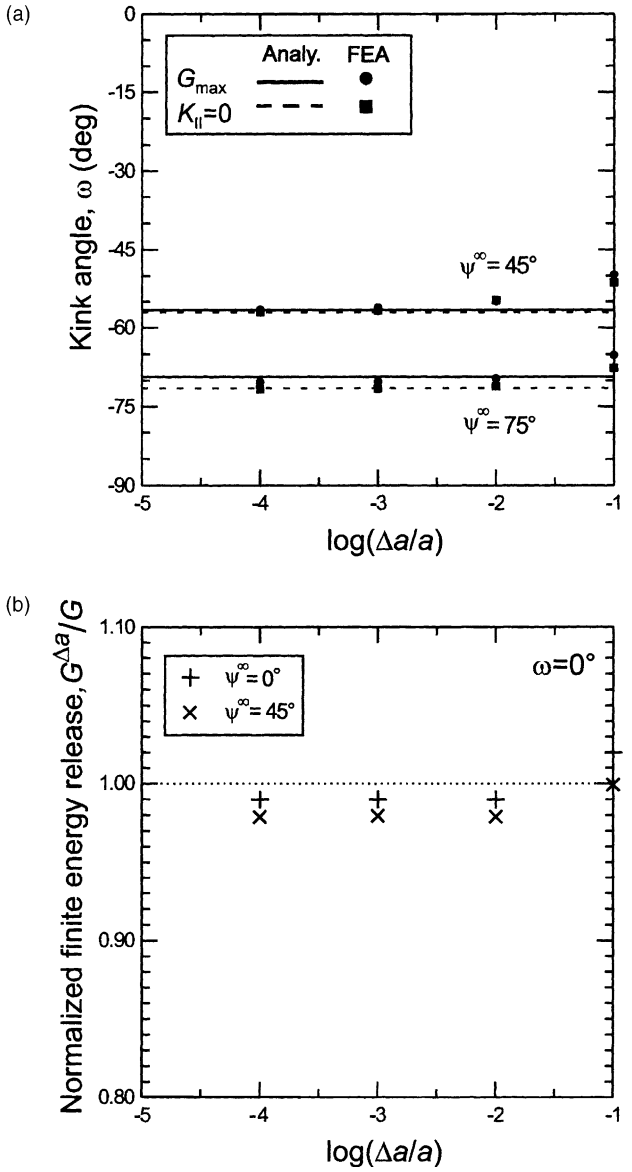

Fig. 5. (a) Optimal kink angles for homogeneous sheet with phase angle $\psi = 45°$ and 75°. The optimal kink angles determined by two criteria and FEA are displayed (closed symbols) and compared with those from the short-kink theories (lines). (b) Finite kink energy release, $G^{\Delta a}$, for $\omega = 0$ normalized by the energy release rate $G = (K_1^2 + K_2^2)^{1/2}/E'$. These measures will agree in a pure K-field. The T-stress in the homogeneous sample causes the deviations for the longer kink lengths.

5.2. Graded material

5.2.1. Kink angles

The optimal kink angles for the graded material predicted by the two criteria are displayed in Fig. 6a for far-field phase angle $\psi^{\infty} = 45°$, 0°, −45°, deformation biaxiality $B_e = 1$, and $E(y)$ with $ba = 100$. Table 1

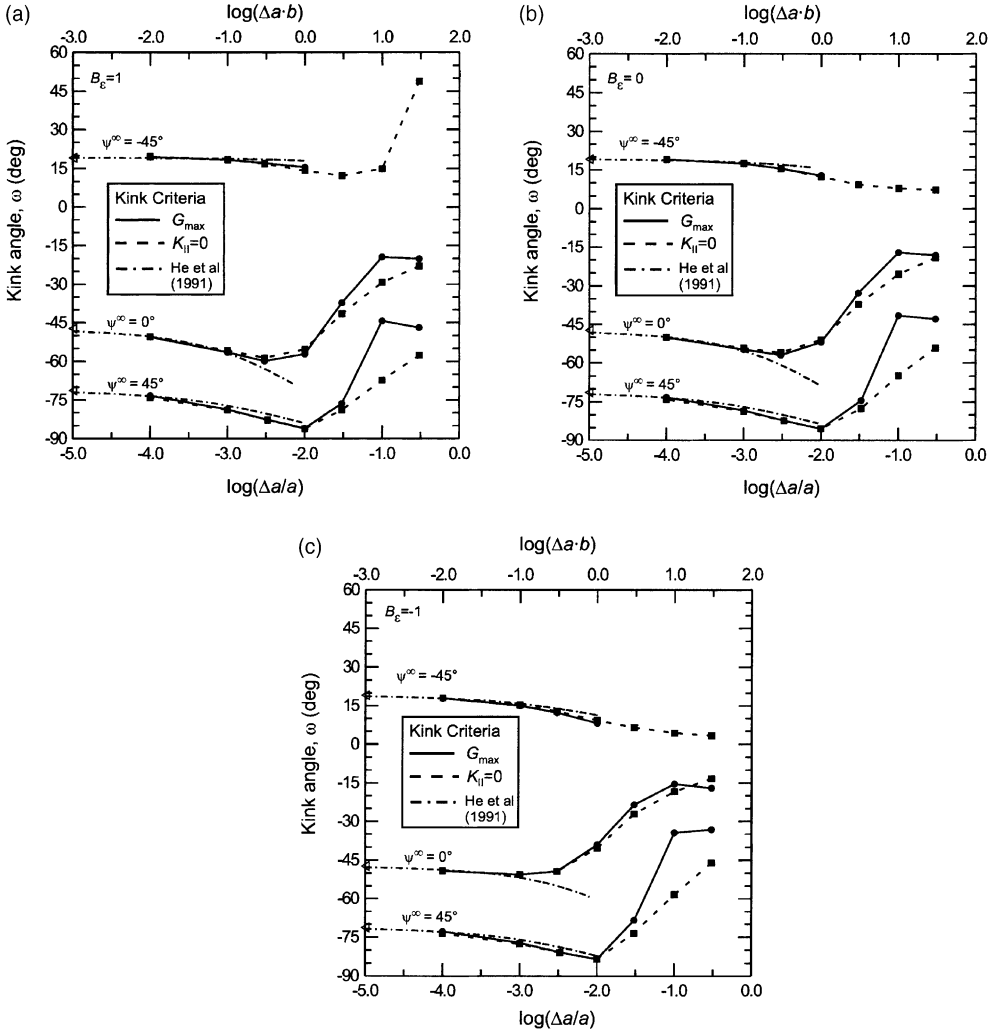

Fig. 6. Optimal kink angle for finite kink length in an FGM with $E(y)$ and deformation biaxiality $B_\varepsilon = 1$ (a), 0 (b) and –1 (c). The asymptotic short kink angle under the $K_{II} = 0$ criterion is displayed as ◁ on the y-axis. The effect of the T-stress is modeled by the analysis of He et al. (1991) for homogeneous materials which depends on $T\sqrt{\Delta a}$. The dependence of kink length for $\Delta a < 1/b$ is found to follow the results of this analysis.

Table 1
Tip parameters for graded sheet

ψ^∞	ψ	$\omega_{G_{max}}(\Delta a \to 0)$	$\omega_{K_{II}=0}(\Delta a \to 0)$	$\omega_{G_{max}}(\Delta a/a = 10^{-4})$	$\omega_{K_{II}=0}(\Delta a/a = 10^{-4})$
−45°	−10°	19.2	19.1	19.4°	19.6°
0°	32°	−46.9	−47.3	−50.6°	−50.5°
45°	75°	−69.3	−71.3	−73.3°	−74.2°

shows the results for the smallest kink calculated $\Delta a/a = 10^{-4}$ and the asymptotic short-kink limit (He and Hutchinson, 1989) (denoted for $\omega_{K_{II}=0}$ by ◁ on the y-axis in Fig. 6a). Even for the shortest kinks analyzed, there is a systematic discrepancy (as much a 4°) from the asymptotic predictions.

As kink lengths increase, the value of the kink angle is found to decrease (become more negative). This trend is steady until roughly $\Delta a/a = 10^{-2}$ (or $\Delta ab = 1$). The effects for even longer kink lengths are twofold: (1) the two criteria drastically diverge, and (2) for most cases the trend in optimal kink angle rapidly becomes less negative (smaller in magnitude).

The first of these effects is due, in part, to the fact that the $K_{II} = 0$ criterion is localized to the tip of the kink, whereas the energy criterion used here depends on the tractions and displacements all along the kink. For cracks in radially self-similar stress fields, there is no change with kink length. However, for longer kinks with lengths comparable to the governing elastic gradient dimension, this no longer holds. The change in the nature of the stress field is due to the modulus gradient. Analogous disparity would be expected in a homogeneous sample for $\Delta a/a \sim 1$.

The effect of biaxiality is displayed in Fig. 6b and c. These show the kink angles for cases with deformation biaxiality $B_\varepsilon = 0$ and –1. The trend in most cases is that the magnitude of kinking is decreased with decreasing biaxiality, B_ε. To the first approximation, this can be understood through the same effect as in the homogeneous case. The application of a far-field compressive stress $\sigma_{xx}^{\infty} < 0$ will decrease the T-stress by $T(\sigma_{xx}^{\infty}) = T(0) + \sigma_{xx}^{\infty}$ and thereby decrease the magnitude of the kink angle. However, this simple relation does not hold for the graded case.

5.2.2. Modulus affected stresses

The change in the stress fields with radial distance from the tip is demonstrated in Fig. 7 for $B_\varepsilon = 0$. This shows FEA results $\{\sigma_{xx}, \sigma_{yy}, \sigma_{\theta\theta}\}\sqrt{(2\pi r)}/|K|$ at distances of $r = 10^{-4}a = 10^{-2}/b$ (a) and $r = 10^{-2}a = 1/b$ (b). With this normalization, the results would be invariant for all r in an infinite homogeneous body. The change in the stress states from those of Fig. 7a to those of Fig. 7b is due to the influence of higher-order gradient- and geometry-dependent terms. For comparison, the results of the Williams' equation (with $\psi = 32°$) are in Fig. 7c. The finite element results agree well with the Williams' field at the smaller dimension, with the most notable exception being an increase in σ_{xx}, attributable to a T-stress. At the larger dimension there are more drastic differences in the fields. Focusing along $\theta = 0°$, there is a larger difference between σ_{xx} and σ_{yy}. In a Williams' field, regardless of phase angle, σ_{xx} and σ_{yy} are the same along $\theta = 0°$. In addition the location of the maximum hoop stress has shifted roughly 40°.

Such a shift motivates a comparison of these results with the analytical description of the stress field in the neighborhood of an interface crack. In the limit of $b \to \infty$, the sigmoidal gradient will form a sharp interface with $E_1(y > 0)$, $E_2(y < 0)$, and $\nu_1 = \nu_2 = \nu$. In the notation of interface mechanics, the oscillatory index, ε, can be calculated in plane strain from the moduli ratio, via:

$$\varepsilon = \frac{1}{2\pi} \ln \left[\frac{(3 - 4\nu) + E_1/E_2}{1 + (3 - 4\nu)E_1/E_2} \right] \tag{10}$$

and for $E_1/E_2 = 20$ and $\nu = 0.3, \varepsilon = -0.084$. The nondimensional Dundurs' parameters (Dundurs, 1969) $\{\alpha, \beta\}$ are $\{0.9, 0.26\}$. Setting the reference phase angle to be the same as for the FGM case at $r = 10^{-4}a$ and using the asymptotic stress solutions for an elastic interface crack (Rice et al., 1990), the results of Fig. 7d are obtained.

The xx-stresses are discontinuous across the interface, but at this distance from the tip in an FGM, the change in properties is still experienced over a number of finite elements and such discontinuities are not exhibited. The trend for larger xx-stresses for $\theta > 0$ is seen in the interface analysis just as in the finite element results for the FGM. Note that the normalized difference between the σ_{xx} and σ_{yy} is greater in the FGM case than predicted by either the homogeneous or interface-crack solutions. [2] For the interface crack solution with $T = 0$, the average of σ_{xx} at 0^+ and at 0^- is equal to σ_{yy}.

[2] For an interface crack there exists a T-stress that is invariant with r, although this term will have two different values above and below the interface. Their relationship is constrained by the compatibility condition on $y = 0$ (Rice, 1998).

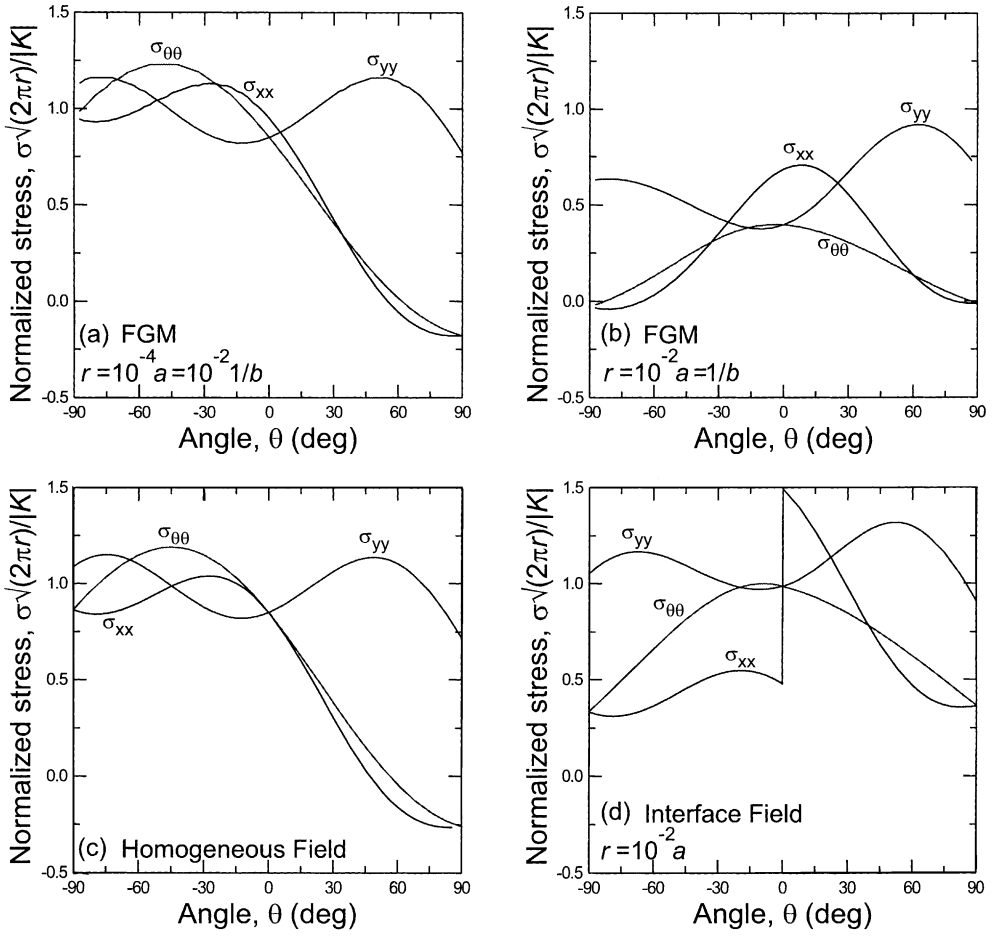

Fig. 7. Stress components calculated at $r = 10^{-2}/b$ (a) and $1/b$ (b) for $\psi^{\infty} = 0°$. At the smaller distance, the finite element results compare well with Williams' field (a). The stresses in (b) are dramatically different, including a shift in the angle of maximum hoop stress, $\sigma_{\theta\theta}$. The analytical stress fields for cracks in homogeneous materials (c) and on bimaterial interfaces (d) for a reference phase angle of 32° (at a reference distance $L = 0.0001a$). For the homogeneous materials, these results are independent of r. For the interface case, r is set to be $100L$, which facilitates comparison with (b). The shift in the angle of maximum hoop stress compares to that in (b), as well does the relative increase in σ_{rr} for $\theta > 0$.

For an elastic interface crack there is a well-known shift in the local phase angle $\psi(r) = \tan^{-1}(\sigma_{xy}/\sigma_{yy})$ with distance ahead of the crack tip. Moving from a reference location, L, to r, the phase angle will be shifted $\psi(r) = \psi(L) + \varepsilon \ln(r/L)$, where ε is the oscillatory index of Eq. (10). It can be seen that the shift in the location of maximum hoop stress is predicted by the interface equations, although with a sharper maximum in $\sigma_{\theta\theta}$ than in the FGM case.

The behavior of the local phase angle, $\tan^{-1}(\sigma_{xy}/\sigma_{yy})$ is illustrated for the FEA calculations for the interface ($b \to \infty$), FGM and homogeneous cases in Fig. 8 for $B_{\varepsilon} = 0$. For the homogeneous case, by symmetry, $\sigma_{xy} = 0$ for all r. The interface results are seen to be parallel to the analytical solution with slope ε for $r < a/10$. At larger dimensions, geometry effects cause small variations from this trend. As expected, the FGM exhibits characteristics of both the interface and the homogeneous case: a region of K-dominance for σ_{xy} and σ_{yy} in the almost homogeneous region near the crack tip and a region of varying $\psi(r)$ at dimensions $r \sim 1/b$.

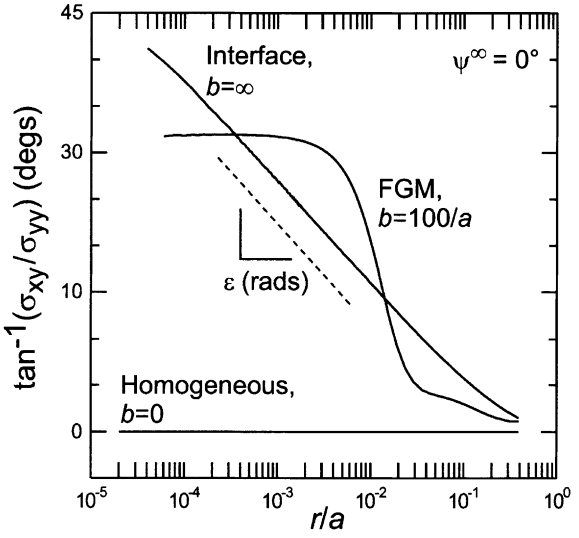

Fig. 8. The local phase angle $\psi(r) = \tan^{-1}(\sigma_{xy}/\sigma_{yy})|_{\theta=0^\circ}$ for the homogeneous ($b = 0$), FGM ($b = 100/a$) and interface ($b \to \infty$) cases for $\psi^\infty = 0$ and $B_\varepsilon = 0$. For the homogeneous body $\psi(r)$ is zero (by symmetry). There is a well-defined region with the calculated phase angle being approximately constant for the FGM case when $r < 1/b$. The shift in $\psi(r)$ for the interface crack is dictated by the value of the oscillatory index, ε.

Thus, it is apparent that the interface mechanics solution captures some of the effect of the gradient at this distance from the crack tip. For sufficiently large bodies and long kinks ($\Delta ab \gg 1$), the distinction between the sharp and the graded sigmoidal interface could be diminished. In this situation, interface fracture mechanics solutions could be applied directly.

5.2.3. Parallel stress calculation

The power-series solution to the homogeneous crack problem (Eq. (2)) indicated that the second term in the stress solution is constant. For free crack faces, the normal and shear tractions must be zero, so the only constant nonzero component must be σ_{xx}. For graded materials, such a constant term is not possible, as a constant stress in a material with varying modulus violates the conditions of compatibility. It suffices to say that the next-order term in the stress solution will be T-like in that the flank boundary conditions still dictate that the effect of the higher-order terms will be strongest in the xx component of stress. To what extent this term for FGMs, denoted T_b, varies has not been established analytically. It also is evident from comparing Fig. 7a and b that there are terms acting on all components of stress within $r < 1/b$.

To attempt to capture the effects of the gradient-induced stresses, the apparent T-stress, $\sigma_{xx} - \sigma_{yy}(\theta = 0)$, was calculated for the FGM cases. These are displayed in Fig. 9a–c for a range of distances from the crack tip. In the homogeneous case, T is independent of ψ^∞. However, just as the tip phase angle is shifted for the FGM case, the parallel stress is shifted as well, with its value adjusted significantly by the far-field phase angle, ψ^∞. It is apparent for each case that sufficiently close to the crack tip ($r < 0.1b$), the apparent T-stress is approximately constant. There are variations (roughly 50% from $r = 10^{-5}a$ to $10^{-3}a$), but given the dominance of the singular components ($\sigma \propto 1/\sqrt{r}$) of the stress field at these dimensions, changes on the order of 1000% are expected. A single asymptotic value for the FGM T-stress, T_b, was defined to be the average over two finite elements as $r \to 10^{-5}a$.

The effect of biaxiality is seen with a nonlinear decrease in the apparent T-stress with decreasing deformation biaxiality (Table 2). For a given ψ^∞, T_b shifts roughly linearly with the nominal far-field stress

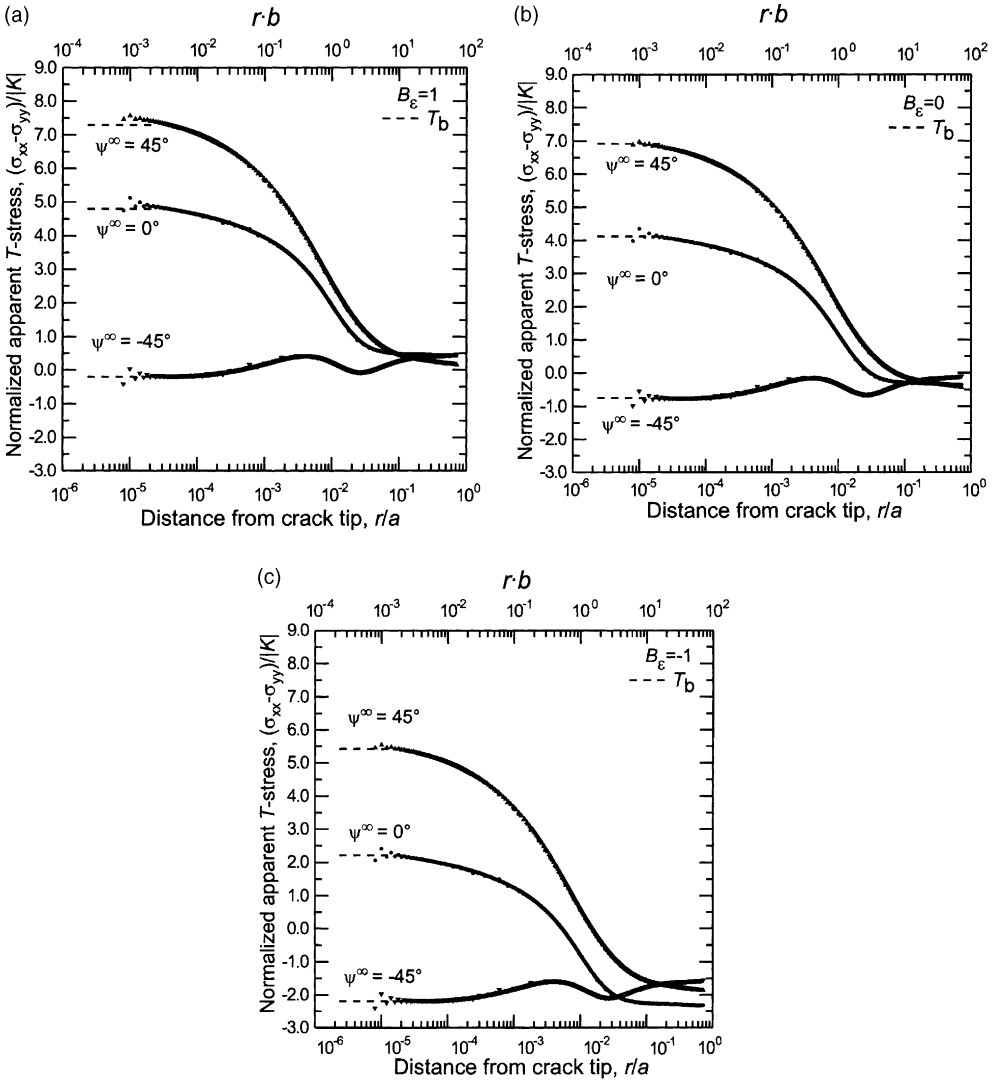

Fig. 9. The apparent T-stress, $\sigma_{xx} - \sigma_{yy}$ along $\theta = 0$ for the FGM sheet with deformation biaxiality $B_\varepsilon = 1$ (a), 0 (b) and –1 (c). When calculated sufficiently close to the crack tip, this value is roughly constant, varying 50% from $r/a = 10^{-5}$ to 10^{-3}, where the singular stress field changes 1000%. However, this asymptotic value, T_b, has a much different value than for a homogeneous sample.

Table 2
Normalized FGM T-stress, $T_b\sqrt{a}/|K|$

ψ^∞	$B_\varepsilon = 1$	$B_\varepsilon = 0$	$B_\varepsilon = -1$
−45°	−0.2	−0.77	−2.2
0°	4.8	4.1	2.2
45°	7.3	6.9	5.4
$b = 0$, $\psi^\infty = 0°$	0.13	−0.20	−1.0

σ_{xx}^∞, although a more thorough exploration of the dependence of T_b on both B_ε and ψ^∞ would be required to establish the explicit dependence.

Thus, it can be seen that there is a gradient induced T-stress that depends strongly on ψ^{∞} and can be much larger than for the homogeneous sample with the same far-field loading. It is of interest to compare the results for a sharp interface ($b \to \infty$) and the same far-field loading. Due to the discontinuity in $E(y)$ for an interface, the FEA stresses on the interface will be prone to error. Extrapolating the stresses as $y \to 0^{+}$ and $y \to 0^{-}$ indicates that for this geometry $T\sqrt{a/|K|} \sim 1$ with a variation of ± 0.5 for $-45° < \psi^{\infty} < 45°$. This value is comparable to the apparent T-stress for the FGM samples analyzed at $rb > 1$ (but at this distance, $r/a > 0.1$, other geometry-dependent higher-order terms are also not trivial). This is much less than in the near homogeneous region, $rb \ll 0.1$, and therefore it is clear that the apparent T-stress for the FGM is larger than for either the homogeneous or interface case.

Combining T_b with the tip phase angle ψ, Eq. (3b) allows a prediction of the dependence of kink angle on kink length expected by the $K_{\mathrm{II}} = 0$ criterion in a homogeneous material (He and Hutchinson, 1989). These predictions are included in Fig. 6 (dashed-dot lines). As expected, these curves asymptote to the short-crack values for small $\Delta a/a$. There is excellent agreement with the prediction for homogeneous materials and the FGM results for small $\Delta a/a$. The agreement ends as $b\Delta a \to 0.1$, where, as discussed, the next-order term not captured by a constant T_b in the stress analysis is expected to begin altering the behavior of the kink.

It is evident that the magnitude of $T_b\sqrt{a/|K|}$ can be much greater for the FGM case than for the homogeneous sample under similar loading. This is particularly true for positive biaxiality and phase angle. Therefore, just as the gradient-induced phase angle dominates for as $\Delta a/a \to 0$, gradient-induced T-stress dominates for $\Delta a < 1/b$.

5.2.4. Bifurcation in energy criterion

The kink angles resulting for the $G_{\max}$ criterion are not displayed in Fig. 6a–c for the $\psi^{\infty} = -45°$ ($(\mathrm{d}E/\mathrm{d}y)\psi < 0$) case and $\Delta a/a > 10^{-3}(\Delta a b > 0.1)$. This is due to a bifurcation in $G^{\Delta a}$, as displayed in Fig. 10. For short kinks $\Delta a/a \leqslant 10^{-2}$, there is a single maximum in $G^{\Delta a}$ vs. ω, as in the homogeneous case.

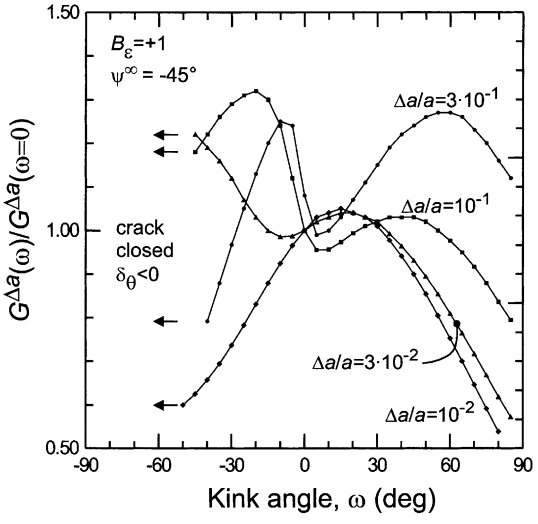

Fig. 10. The variation of the finite kink energy release, $G^{\Delta a}$, for a range of kink angles, ω, normalized to $G^{\Delta a}$ ($\omega = 0$). For these, deformation biaxiality, $B_{\varepsilon} = 1$ and far-field phase angle $\psi^{\infty} = -45°$. For the shortest kink displayed, $\Delta a/a = 10^{-2}$, there is a single maximum, as in homogeneous materials. The competition between the far-field loading and gradient-induced effects leads to multiple stationary points for longer kinks.

However, it is evident that kinking down into increasingly compliant material as $\omega < 0°$ is conducive to increasing values of energy release in a direction not predicted by either the far field or tip phase angles. Note that for fixed K, the analytic expression $G = |K|^2/E'$ predicts an inverse relationship between energy release rate and elastic stiffness.

This behavior is limited to the $\omega_{G_{\max}}$ criterion, as the kinks below 0° are subject to a high amount of shear and only a single $\psi^{\text{kink}} = 0$ angle is found, as displayed in Fig. 6. Beyond $\omega = 45$–$60°$ the kink closes ($\delta_\theta = 0$) and the energy release is due entirely to sliding opening, δ_r. For kink angles beyond this limit, the crack faces come into contact. If detailed results of crack behavior in this regime were to be studied, then a contact-element routine would be required. This is beyond the scope of the present investigation.

It is apparent that for kinks of sufficient length there is a competition between the traditional near-tip driving force and that energy release available by growing the crack in shear into the very compliant region. Negative far-field loading drives the crack up into the stiffer material and the compliance effects are of opposite direction. Naturally, for conditions of positive tip phase angle ($(\mathrm{d}E/\mathrm{d}y)\psi > 0$; e.g. $\psi^\infty = 0°, 45°$), the driving forces compliment each other, rather than compete, and this bifurcation is not observed.

The bifurcation in results also arises for the case of pure transverse tensile deformation, $\varepsilon_{yy}^\infty = \varepsilon_{xy}^\infty = 0$, $\varepsilon_{xx}^\infty = 1$. This results in a tip phase angle $\psi = 31.5°$ and $T_b\sqrt{a}/|K| = 6.7$. The finite energy release for kinks normalized by the energy release for a crack along $\omega = 0°$ is displayed in Fig. 11a. For the short kinks, $\Delta a/a \leqslant 10^{-2}$, $\Delta ab \leqslant 1$, the maximum release angles are single valued. For longer kinks, there is a tendency for an increased energy release as $\omega \to 90°$. The phase angles at the tip of the kink are displayed in Fig. 11b. There is a similar trend, with multiple angles corresponding to $K_{\text{II}} = 0$. These have a close correspondence with the results of the $G_{\max}$. The $\omega_{K_{\text{II}}=0}$ values are indicated by $\downarrow$ in Fig. 11a. For $\Delta a/a = 10^{-4}$, this closely corresponds to $\omega_{G_{\max}}(\partial G/\partial\omega = 0, \partial^2 G/\partial\omega^2 < 0)$. However, it is apparent there are a number of angles for which the kink phase angle is zero, but the energy release is a nearly local *minimum* ($\partial G/\partial\omega = 0, \partial^2 G/\partial\omega^2 > 0$). It is apparent that not only the zero point for K_{II}, but also the derivative $\partial K_{\text{II}}/\partial\omega > 0$ needs to be satisfied for the optimal kink angle.

5.3. Extension conditions

Even with a full accounting for the effect of a modulus gradient on a crack path in an FGM, accurate modeling of the fracture behavior requires additional analysis. For sharp interfaces, the balance of the mechanical driving force and the relative toughness determines the direction of crack propagation. For the crack to kink off the interface and into the substrate (along ω), the criterion $G(\omega)/G_{\text{c}}^{\text{sub}} > G(0)/G_{\text{c}}^{\text{if}}$ (where $G_{\text{c}}^{\text{sub}}$, G_{c}^{if} are the toughness, in terms of energy release rate, of the substrate and the interface) has been established (He et al., 1991). In general, the fracture toughness of a continuously inhomogeneous material will also vary with direction. This may be due to variance in the composite surface energy, Γ, and atom trapping for an elastic material or the yield strength for an elastic–plastic material. Therefore, a similar competition between regions of higher stress (or potential energy release rate) and lower material resistance need be established. The domains in which each of these effects are dominant, or are in competition, must be determined in order to successfully predict the experimental fracture behavior.

6. Summary

Established theories for the in-plane kinking of a mixed-mode crack use the tip phase angle to determinate the optimal angle. For homogeneous materials, the $K_{\text{II}} = 0$ and $G_{\max}$ criteria agree within 3° for all but the most extreme kink angles. There is an additional effect of the parallel T-stress, which will increase the magnitude of kinking when positive and inhibit kinking when negative. Even for very short kinks in FGMs (those such that $\Delta a/a \leqslant 10^{-4}$, $\Delta ab \leqslant 10^{-2}$), the optimal kink angle predictions based only on tip

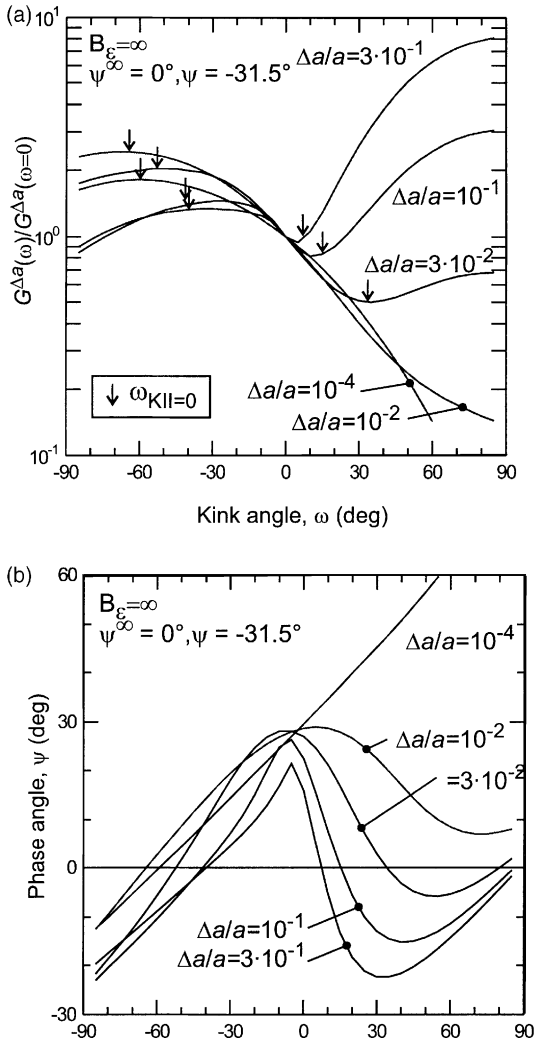

Fig. 11. The bifurcation in fracture parameters in the case of pure tensile deformation in the x-direction, $B_{\varepsilon} = \infty$, $\psi^{\infty} = 0$. For the short kinks, $\Delta a/a \leqslant 10^{-2}$, $\Delta ab \leqslant 1$, the optimal kink angles are single-valued, with close correspondence between the results of the $G_{\max}$ and $K_{II} = 0$ criteria (identified in (a) by ↓). For longer kinks there are multiple solutions to either criteria.

phase angle disagree with finite element results by as much as 4°. For kink lengths within $\Delta a < 1/b$, this disparity and the dependence of kink angle on kink length is well modeled by calculating the apparent gradient-induced T-stress and using it to calculate the conditions at the kink tip. It was found that this T-stress depends on the far-field xx stress and even more strongly on the far-field phase angle. It can be much larger for the FGMs studied than for a homogeneous material with the same geometry and loading. This gradient induced T-stress is large in a region of size similar to that of the gradient dimension $rb < 1$, and can significantly exceed the value for a sharp interface with the same loading. For a positive apparent T-stress, the crack path is less stable, with the crack closely following the asymptotic small kink angle predictions only for $\Delta a/a < 10^{-3}$. Outside of the gradient dimension, $1/b$, there is a drastic effect of kink length including a widened divergence between the predictions based on energy maximization ($G_{\max}$) and on kink

symmetry ($K_{II} = 0$). These effects cannot be characterized in terms of stress intensity factors or analyses that include an additional constant parallel stress.

Acknowledgements

Work supported by the Director, Office of Science, Office of Basic Energy Sciences, Materials Sciences Division of the US Department of Energy under contract no. DE-AC03-76SF00098.

References

Cotterell, B., 1965. On brittle fracture paths. Int. J. Fract. Mech. 1, 96–103.
Cotterell, B., 1966. Notes on the paths and stability of cracks. Int. J. Fract. 2, 526–533.
Cotterell, B., Rice, J.R., 1980. Slightly curved or kinked cracks. Int. J. Fract. 16, 155–169.
Dundurs, J.J., 1969. Edge-bonded dissimilar orthogonal elastic wedges under normal and shear loading. J. Appl. Mech. 36, 650–652.
Erdogan, F., 1995. Fracture mechanics of functionally graded materials. Compos. Engng. 5, 753–770.
Erdogan, F., Sih, G.C., 1963. On the crack extension in plates under plane loading and transverse shear. J. Basic Engng. 85, 519–527.
Finnie, I., Saith, A., 1973. A note on the angled crack problem and the directional stability of cracks. Int. J. Fract. 9, 484–486.
Geubelle, P.H., Knauss, W.G., 1995. Crack propagation in homogeneous and bimaterial sheets under general in-plane loading: nonlinear analysis. J. Appl. Mech. 62, 601–606.
Gu, P., Asaro, R.J., 1997. Crack deflection in functionally graded materials. Int. J. Solids Struct. 34, 3085–3098.
Hayashi, K., Nemat-Nasser, S., 1981. Energy-release rate and crack kinking under combined loading. J. Appl. Mech. 48, 520–524.
He, M.-Y., Hutchinson, J.W., 1989. Kinking of a crack out of an interface. J. Appl. Mech. 56, 270–278.
He, M.-Y., Bartlett, A., Evans, A.G., Hutchinson, J.W., 1991. Kinking of a crack out of an interface: role of in-plane stress. J. Am. Ceram. Soc. 74, 767–771.
Hutchinson, J.W., Suo, Z., 1991. Mixed-mode cracking in layered materials. Adv. Appl. Mech. 29, 63–191.
Jin, Z.-H., Noda, N., 1994. Crack-tip singular fields in nonhomogeneous materials. J. Appl. Mech. 61, 738–740.
Jin, Z.-H., Batra, R.C., 1996. Some basic fracture mechanics concepts in functionally graded materials. J. Mech. Phys. Solids 44, 1221–1235.
Knott, J.F., 1973. Fundamentals of Fracture Mechanics. Butterworths, London.
Konda, N., Erdogan, F., 1994. The mixed mode crack problem in a nonhomogeneous elastic medium. Engng. Fract. Mech. 47, 533–545.
Lee, Y.-D., Erdogan, F., 1995. Residual/thermal stresses in FGM and laminated thermal barrier coatings. Int. J. Fract. 69, 145–165.
Palaniswamy, K., Knauss, W.G., 1978. On the problem of crack extension in brittle solids under general loading. In: Namat-Nassar, S. (Ed.), Mechanics Today, vol. 4. Pergamon Press, New York.
Rice, J.R., 1988. Elastic fracture mechanics concepts for interfacial cracks. J. Appl. Mech. 55, 98–103.
Rice, J.R., Suo, Z., Wang, J.-S., 1990. Mechanics and thermodynamics of brittle interfacial failure in bimaterial systems. In: Rühle, M., Evans, A.G., Ashby, M.F., Hirth, J.P. (Eds.), Metal–Ceramic Interfaces, Pergamon Press, Oxford, p. 269-94.
Williams, M.L., 1957. On the stress distribution at the base of a stationary crack. J. Appl. Mech. 79, 109–114.
Williamson, R.L., Rabin, B.H., Byerly, G.E., 1995. FEM study of the effects of interlayers and creep in reducing residual stresses and strains in ceramic–metal joints. Compos. Engng. 5, 851–863.
Zienkiewicz, O.C., Taylor, R.L., 1989. The Finite Element Method. McGraw-Hill, New York.